Directional resolution of the GaAs heavy-hole band dispersion and photoelectron-momentum orientation from hot-electron luminescence

W. Hackenberg and H. P. Hughes
University of Cambridge, Cavendish Laboratory, Cambridge CB3 0HE, United Kingdom
(Received 13 September 1993)

It is demonstrated how the heavy-hole dispersion of bulk GaAs can be obtained along specific high-symmetry directions from hot-electron to neutral acceptor photoluminescence spectroscopy. This is done by analyzing the degree of linear polarization in terms of a detailed line-shape calculation to identify that part of the emission which is due to carriers with a particular wave-vector direction. A systematic plot of $E_h(\boldsymbol{k})$ with sub-meV accuracy is thus made possible over a range of wave vectors in the central Γ valleys of direct-gap semiconductors. This method exploits the hot-electron momentum orientation by linearly polarized light, which is systematically investigated, together with the extent to which such momentum orientation persists in a hot-electron population either after one-phonon emission or when it is subjected to significant carrier-carrier scattering.

I. INTRODUCTION

Hot-electron to neutral acceptor photoluminescence spectroscopy can produce interesting insights into hot-electron dynamics of direct-gap III-V semiconductors because the cw (e, A^0) spectrum represents a direct record of the steady-state electron distribution in the conduction band.[1,2] Due to the low incident laser power a very good spectral resolution is achieved. This in turn makes it possible to analyze the line shape of the (e, A^0) emission which contains a wealth of information on ultrafast scattering processes[3] and on the band structure of the semiconductor material.[4,5] For a detailed understanding of the physics involved, a model was developed to calculate such line shapes in great detail; it incorporates a $\mathbf{k}\cdot\mathbf{p}$ band-structure calculation and evaluates optical transition matrix elements in the dipole model.

This paper focuses on two areas. First, an observation of the phenomenon of hot-electron momentum orientation by linearly polarized light is systematically investigated and explained in detail (Sec. III). This phenomenon was predicted by Dymnikov, Dyakonov, and Perel.[6] Good conditions for observing this effect in direct-gap semiconductors exist in a low-power and low-temperature cw measurement of (e, A^0) photoluminescence (PL) at excitation energies between 1.6 and 1.8 eV, when the photoexcited electrons are both below the $\Gamma \rightarrow L$ intervalley scattering threshold and out of the range of thermalized electrons. Then perturbation by hot phonons, a background plasma or transient phenomena is negligible, and a detailed study of the sensitivity of hot (e, A^0) PL to polarized excitation is possible; here the line-shape calculation mentioned above proves to be a very useful tool for analysis and interpretation. This understanding is subsequently used to investigate how carrier-carrier scattering and phonon scattering affect the momentum orientation within a hot-electron population (Sec. V).

Second, it is demonstrated how the heavy-hole dispersion in GaAs may be obtained along specific high-symmetry directions from hot (e, A^0) PL spectroscopy (Sec. IV). Indeed, such measurements cannot distinguish between emission from carriers with particular momentum directions without extra theoretical input. While effective-mass values are often determined[7] near the zone center, the dispersion of the Γ_8^v and Γ_7^v bands in bulk GaAs has been determined away from it over a relatively wide range of wave vectors from (e, A^0) spectra,[4] but directional resolution could not be achieved at the time. In quantum wells, this problem is made easier by the restriction to two dimensions.[8] In bulk, it has so far only been possible to extract directional information by elimination of emission from carriers with particular $\mathbf{k}$ directions.[5] In this paper, we demonstrate a method of analyzing hot (e, A^0) spectra in such a way as to obtain the dispersion of the heavy-hole (HH) band along approximate and along specific high-symmetry directions, namely [100] and [111].

II. TECHNIQUE AND THEORY

Hot (e, A^0) luminescence, also called hot-electron luminescence (HEL), is schematically illustrated in Fig. 1.[2] Upon cw photoexcitation, one has $E_{ex} = E_h(\mathbf{k}) + E_0 + E_c(\mathbf{k})$, where E_{ex} is the laser energy, $E_h(\mathbf{k})$ the heavy-hole energy, E_0 the low-temperature band gap at $\mathbf{k}=0$, and $E_c(\mathbf{k})$ the hot-electron energy (direct transitions). Upon immediate recombination, i.e., prior to any phonon emission, the luminescence energy is $E_L = E_c(\mathbf{k}) + E_0 - E_a$. The acceptor binding energy E_a is independent of $\mathbf{k}$ because the acceptors are localized at $p < 10^{17}\ \mathrm{cm}^{-3}$. This allows the determination of the energies of both the hot electron and the photocreated hole in terms of quantities easily accessible from experiment: $E_c(\mathbf{k}) = E_L - E_0 + E_a$ and $E_h(\mathbf{k}) = E_{ex} - E_L - E_a$. This memory of the hole state before excitation exists only in the first HEL peak. The corresponding wave vector is not directly accessible with this technique but can be found using known dispersion relations of the conductions band (for example, parabolic with known effective

mass, or from Ref. 9). The photoexcited hot electrons relax toward the bottom of the band by successive emission of LO phonons on a 100 fs time scale, while optical recombination occurs on a 1 ns time scale. The (e, A^0) spectrum thus provides a direct record of the hot-electron relaxation process. Figure 2 shows an example of this so-called hot-electron cascade.

In the following we will focus on the leading peak in this cascade. The line shape of this hot (e, A^0) emission may be calculated[2] for a given E_{ex} with the "golden rule":

$$I(E_L)=\int_{\text{Brillouin zone}} d\mathbf{k}|M_{vc}(\mathbf{k})|^2|M_{ca}(\mathbf{k})|^2\delta[E_{ex}-E_c(\mathbf{k})-E_h(\mathbf{k})-E_0]\delta[E_L-E_h(\mathbf{k})-E_0+E_a]\ . \quad (1)$$

$I(E_L)$ is the total luminescence intensity expected in the (e, A^0) spectrum at the energy E_L. Energy conservation for excitation and recombination is ensured in the two δ functions. $E_v(\mathbf{k})$ and $E_c(\mathbf{k})$ are measured positive from their band extrema. For the band structure a 16×16 $\mathbf{k}\cdot\mathbf{p}$ Hamiltonian is used;[10] it is important that spin-orbit interactions, nonparabolicity, and warping be taken into account when investigating line shapes and polarization effects in any detail. The optical transition matrix elements $|M_{vc}(\mathbf{k})|^2$ for excitation and $|M_{ca}(\mathbf{k})|^2$ for recombination are calculated in the dipole approximation and depend on the polarizations $\mathbf{e}$ and $\mathbf{e}'$ of the in-going and out-going light, and on the magnitude and orientation of $\mathbf{k}$. Equation (1) is central to the present line-shape model. It yields the spectral (e, A^0) luminescence profile as it results from the specific band structure and the interaction between light and the electron states in the dipole model. Broadening effects, mainly lifetime broadening, are included subsequently by convolving the resulting profile with a Lorentzian to fit the measured line shape [cf. Fig. 4(a) below].

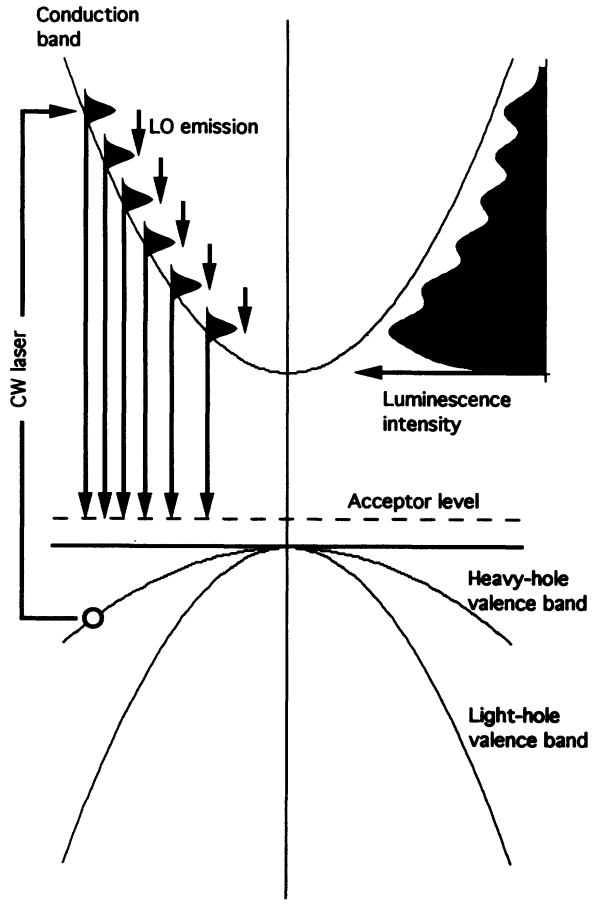

FIG. 1. Schematic of cw electron luminescence spectroscopy in lightly p-doped GaAs (after Ref. 2). The vertical arrow on the left represents laser excitation of electrons from the heavy-hole band into hot conduction-band states with $E_c(\mathbf{k})\gg k_BT$. Relaxation is via emission of a cascade of LO phonons in successive steps of energy $\hbar\omega_{LO}$. Since recombination during this process is with an acceptor of $\mathbf{k}$-independent energy, the (e, A^0) spectrum exhibits a "hot-electron cascade" superposed on the rising exponential tail of the band-gap luminescence.

III. OPTICAL ORIENTATION OF HOT-ELECTRON MOMENTA

This section explains the theory of the orientation of hot-electron momenta by excitation with linearly polarized light. The expectations thus derived are then compared with actual observation. In Eq. (1), the energy of any observed luminescence depends on E_{ex} and on the band structure, whereas the intensity of any optical transitions is given by the optical matrix elements. We are interested in the relationship between the polarization of the exciting (and detected) light and the momentum $\mathbf{k}$ of the excited (and radiatively recombining) hot electron.

The matrix elements for optical transitions between hole and conduction states were derived in Ref. 2. Pure

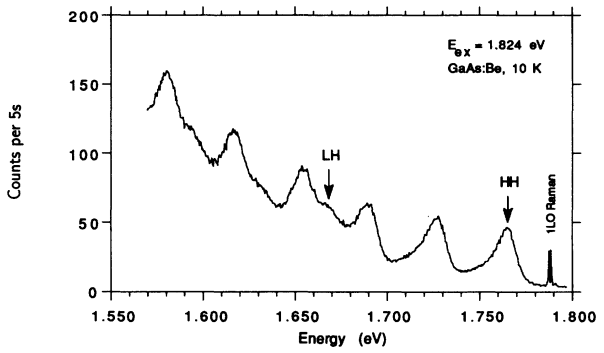

FIG. 2. HEL spectrum showing the cascade of hot electrons relaxing via LO-phonon emission. HH denotes the succession of six peaks, spaced by about $\hbar\omega_{LO}$, which trace the relaxation of hot electrons excited out of the heavy-hole band; similarly LH denotes three shoulders, tracing electrons from the light-hole band. The Raman line is $\hbar\omega_{LO}$ below the laser line. The first peak in each series is due to carriers recombining before any phonon emission.

and spherically symmetric wave functions were assumed, and the correspondence principle was invoked to treat optical interband transitions as oscillating, classical dipoles that couple with the electric-field vector of the photon. The square of the amplitude of the dipole moment $\langle m|\hat{\mathbf{D}}|n\rangle$, where $\hat{\mathbf{D}}$ is the dipole moment operator, represents the probability of the corresponding interband transition. For transitions between heavy-hole states $m_j=\pm\frac{3}{2}$ and conduction states $s=\pm\frac{1}{2}$ the nonvanishing matrix elements were found to represent circularly rotating dipoles:

$$\begin{aligned}
&\langle m_j=+\tfrac{3}{2}|\hat{\mathbf{D}}|s=+\tfrac{1}{2}\rangle=-\frac{1}{\sqrt{2}}(\lambda+i\mu)\,,\\
&\langle m_j=-\tfrac{3}{2}|\hat{\mathbf{D}}|s=-\tfrac{1}{2}\rangle=+\frac{1}{\sqrt{2}}(\lambda-i\mu)\,,\\
&\langle m_j=\mp\tfrac{3}{2}|\hat{\mathbf{D}}|s=\pm\tfrac{1}{2}\rangle=0\,,
\end{aligned}\tag{2}$$

where λ and μ are orthonormal vectors in the plane perpendicular to the electron momentum $\mathbf{p}$. An excitation, therefore, takes place with maximum likelihood if the electric-field vector $\mathbf{e}$ of the incoming photon lies in the plane of λ and μ in which the dipole representing the transition is rotating. This is the case for all electron momenta $\mathbf{p}$ forming an angle $\theta=90°$ with $\mathbf{e}$, and the transition does not occur for electrons with momenta parallel to $\mathbf{e}$ ($\theta=0°$). Both transitions allowed according to Eq. (2) take place with equal probability. When the laser photons are linearly polarized, the photoexcited electron distribution $F(\mathbf{p})$ is highly anisotropic. It will be proportional to the component of $\mathbf{e}$ that lies within the plane perpendicular to $\mathbf{p}$, so that $F(\mathbf{p})\propto\sin^2\theta$. Specifically, when say $\mathbf{e}\|y$ it has the shape of a disc in the xz plane, rotationally symmetric about the y axis, with its center at the origin, and its cross section resembling a figure eight; it is drawn schematically in Fig. 3. This is because in general $F(\mathbf{p})$ contains as a factor the second Legendre polynomial $P_2(\cos\theta)$.[6] Thus, linear polarization is expected to align electron momenta in the plane perpendicular to its electric-field vector.

This initial anisotropic distribution $F(\mathbf{p})$ is of finite duration, as the electrons become subjected to various scattering processes that tend to randomize their momentum directions. However, during the first 200 fs following photocreation, i.e., before phonon emission occurs and if carrier-carrier scattering and impurity scattering are minimal, the initial anisotropy of the momentum distribution largely survives (Sec. V). From the initial states, recombination takes place with acceptor bound holes, whose wave functions are spherically localized and have the same $m_j=\pm\frac{3}{2}$ character as those of the heavy-hole band.[5,11] Accordingly, the (e,A^0) recombination photoluminescence sampling the hot-electron population is also polarized in the plane perpendicular to the recombining carriers' momenta. Before discussing the measurement of Fig. 4(a), we derive the spectrum from theory.

Considering excitation and recombination as two independent processes of the same nature, the intensity of

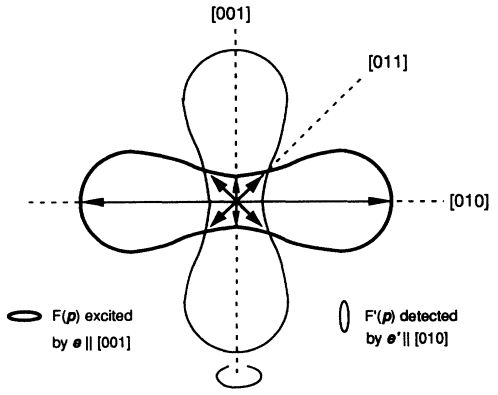

FIG. 3. Cross section through the disc-shaped distribution (bold and rotationally symmetric about the [001] axis) of electron momenta excited by photons with electric-field vector $\mathbf{e}\|[001]$: electrons with $\mathbf{p}\perp\mathbf{e}$ have highest probability for excitation. Arrows represent wave vectors. When detection is with $\mathbf{e}'\|\mathbf{e}$, recombination from electrons with $\mathbf{p}$ oriented in the same bold disc is observed. When detection is with $\mathbf{e}'\|[010]$, only electrons with $\mathbf{p}\perp[010]$ are likely to contribute to the detected signal and only the overlap between the two discs is actually observed.

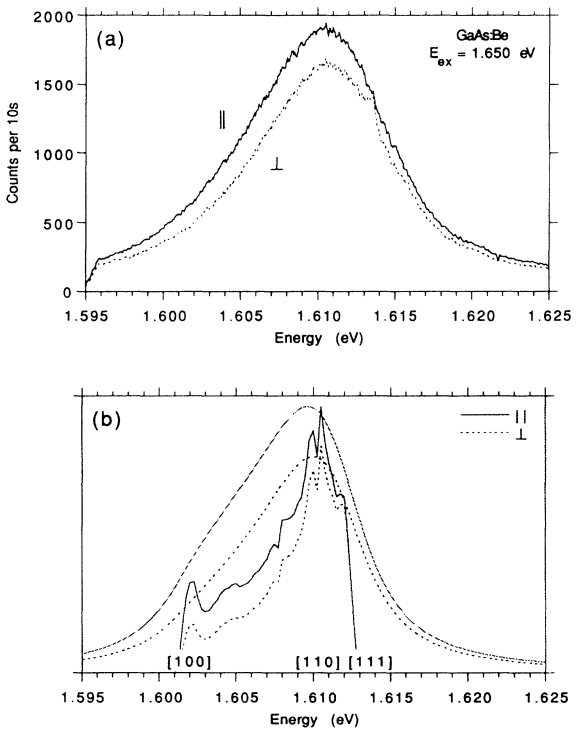

FIG. 4. (a) HEL spectra of the first peak in the cascade measured in a $\bar{x}(yy)x$ geometry for $I_\parallel$ and $\bar{x}(zy)x$ for $I_\perp$ with $x\|[100]$. The 1LO-Raman signal near 1.6134 eV labels the dashed line as the spectrum taken with $\mathbf{e}\perp\mathbf{e}'$. $T<10$ K. (b) The jagged lines represent the (e,A^0) profiles calculated for the conditions in (a) using Eq. (1) before broadening. Due to the HH anisotropy electrons with $\mathbf{k}\|[100]$ directions account for the low-energy end and [111] electrons for the high-energy end; [110] electrons account for the peak. After broadening with a Lorentzian the smooth shapes are obtained. The agreement with (a) in both relative intensities and shape throughout the entire peak profiles confirms the theoretical model.

luminescence emitted with linear polarization $\mathbf{e}'$ at an angle θ' with electron momenta along $\mathbf{p}$, by a population with momentum distribution $F(\mathbf{p})$, is given by:

$$I_{\mathbf{e}'} \propto \int F(\mathbf{p}) \sin^2\theta' d\Omega' , \tag{3}$$

where the integration extends over all angles θ'. Substituting $F(\mathbf{p}) \propto \sin^2\theta$ we have

$$I_{\mathbf{e}'} \propto \int \sin^2\theta \sin^2\theta' d\Omega\, d\Omega' , \tag{4}$$

where the two integrations are over all possible angles θ and θ', representing the angles $(\mathbf{e},\mathbf{p})$ and $(\mathbf{p},\mathbf{e}')$, respectively.[6] It is necessary here to consider all $\mathbf{p}$ because measurements of hot (e, A^0) do not *a priori* discriminate between directions. According to Eq. (4), the integrated spectral intensity $I_\parallel$ of the luminescence polarized parallel to the incident laser ($\mathbf{e}'\parallel\mathbf{e}$) is $32\pi/15$ in arbitrary units, and the integrated spectral intensity $I_\perp$ of the luminescence polarized perpendicular to the laser ($\mathbf{e}'\perp\mathbf{e}$) is $8\pi/5$. As a result the ratio of the integrated luminescence intensities $I_\parallel/I_\perp$ between the two respective configurations is $\frac{4}{3}$. The degree of linear polarization $\eta=(I_\parallel-I_\perp)/(I_\parallel+I_\perp)$, when one takes the integrated spectrum of the first HEL peak for each configuration, is $\eta=1/7$. If one is interested in the relative intensities emitted from electrons traveling along some *specific* high-symmetry directions, then one obtains the following: $\eta_{[100]}=\frac{1}{3}$, $\eta_{[110]}=\frac{1}{11}$, and $\eta_{[111]}=0$.

This may be seen in the two jagged profiles in Fig. 4(b), which shows the result of our calculation based on Eq. (1), integrating numerically over k space, for the two optical configurations above: $I_\parallel$ means $\mathbf{e}'\perp\mathbf{e}\parallel[100]$, $\mathbf{I}_\perp$ means $\mathbf{e}'\perp\mathbf{e}\parallel[100]$. They contain all the information on the $\mathbf{k}\cdot\mathbf{p}$ bands involved and the optical transition matrix elements consistent with the theory laid out above, and serve as the basis for Lorentzian broadening; they represent the starting point for the interpretation of the experimental results below. The luminescence obtained with $\mathbf{e}'\parallel\mathbf{e}$ is significantly more intense than that observed for $\mathbf{e}'\perp\mathbf{e}$, this difference arising asymmetrically on the low-energy side. Because of the lighter effective hole mass along the [100] directions than along [111], the low-energy end of the intensity distribution is due to electrons with $\mathbf{k}\parallel[100]$: here the intensity is halved when $\theta'\rightarrow 90°$, whereas the emission from [111] electrons at the high-energy end remains unaffected. This agrees with the mentioned values for the degree of linear polarization: at 1.602 eV $\eta_{[100]}=\frac{1}{3}$, at 1.6105 eV $\eta_{[110]}=\frac{1}{11}$, and above 1.612 eV $\eta_{[111]}=0$, and for the integrated intensities $\eta=\frac{1}{7}$. A key point here is that these values of η actually identify the energies at which emission from electrons with specific momentum directions occur; we return to this important point later. After suitable broadening with a Lorentzian, one obtains the smooth curves in the same Fig. 4(b): our calculation thus predicts two markedly different line shapes for the two orientations of polarization. As can be seen in Fig. 4(a), the corresponding measurements give a very good confirmation of this prediction.

The spectra of Fig. 4(a) were taken for $E_{ex}=1.650$ eV ($\lambda=751.43$ nm), when $E_c\approx 120$ meV and $k\approx 0.04(2\pi/a)$. The difference between the two configurations $\bar{x}(yy)x$ and $\bar{x}(zy)x$ with $x\parallel[100]$ was created simply by rotating the polarization of the light incident on the sample by 90° and exploiting the high linear polarization sensitivity of the spectrometer. At this regime of photoexcitation density ($\approx 10^{15}$ electrons cm^{-3}) intensity scales linearly with incident power, and carrier-carrier scattering is negligible.[12] The intensity ratio at peak is 1.2, confirming the expected $\eta=\frac{1}{11}$ at this point in the spectrum. Using the entire integrated intensities $\eta=9\%$, which compares favorably with the theoretical value of $\eta=\frac{1}{7}$ given some laser drift and other PL background. The Raman peak superimposed on the $I_\perp$ profile but not on $I_\parallel$ confirms that a degree of 100% linear polarization was incident onto the sample. The peak widths differ on the low-energy side by a measured Δ (FWHM)$=(0.8\pm 0.1)$ meV (FWHM is the full width at half maximum), compared with the 0.9 meV in the calculated shapes.[13] The fact that the measured spectra almost overlap at the plot limit on the left-hand side proves that differences in width cannot be due to carrier-carrier scattering. Remarkable agreement exists indeed between the theoretically predicted line shapes and the actual measurement.

Two conclusions follow from Figs. 4(a) and 4(b). First, the measurements are both qualitatively and quantitatively entirely consistent with the argument made above about the alignment of hot-electron momenta by linearly polarized photons. It was checked that other, physically inequivalent optical configurations do not give equivalent results. Thus, after its prediction[6] the orientation of hot-electron momenta has now actually been observed. Second, the present understanding and calculation of hot (e, A^0) luminescence is fully confirmed. Only for wave vectors larger than 5% of the distance $\Gamma\rightarrow X$, corresponding to $E_{ex} > 1.750$ eV, are the $\mathbf{k}\cdot\mathbf{p}$ parameters found to be inaccurate on a sub-meV scale.[13] A reliable model is thus available for detailed studies of hot photoexcited electrons during the initial 200 fs of their lifetime. Section IV illustrates for GaAs how it may be used to obtain information on the anisotropy of the heavy-hole dispersion.

IV. DIRECTIONAL RESOLUTION OF THE HEAVY-HOLE DISPERSION

This section demonstrates for GaAs a method of analyzing hot (e, A^0) spectra in such a way as to obtain the dispersion of the heavy-hole band both *approximately* along and *exactly* along some high symmetry directions. The hot (e, A^0) emission spectrum can in fact be deconvolved into contributions from different momentum directions. This is demonstrated here in four steps with increasing levels of directional resolution, eventually by determining points on the HH-dispersion along specifically the [100] direction and in principle also along the [111] and [110] directions. For illustration we use one set of spectra obtained with $E_{ex}=1.650$ eV, corresponding to a kinetic hot-electron energy of ≈ 120 meV and $k\approx 0.04(2\pi/a)$, but the same arguments apply in principle for hot-electron states anywhere in the central

Γ valley; however, close to $\mathbf{k}=0$ band gap related PL makes hot PL measurements difficult, and at large $\mathbf{k}$ the $\mathbf{k}\cdot\mathbf{p}$ based model becomes inaccurate.

The following four subsections differ in their identification of a luminescence energy to be associated with the emission from recombining hot electrons with particular momentum directions. Once this E_L, and hence $E_h(\mathbf{k})$, is identified, the same method is used to determine the wave vector $|\mathbf{k}|$ corresponding to this energy (cf. Sec. II), so that the obtained dispersion curves may be compared in one plot. The *direction* that this value of $|\mathbf{k}|$ belongs to, and therefore, the direction of the dispersion on which the so-determined coordinate $(\mathbf{k},E_h(\mathbf{k}))$ lies, is subject of the following discussions.

A. The HH-dispersion approximately along [110]

As may be seen in Fig. 4(b), the maximum of the calculated unbroadened hot luminescence profile results from [110] emission (henceforth this phrasing refers to the carrier momentum not the light geometry). At this point in the profile the degree of polarization equals the theoretically predicted value $\eta=\frac{1}{11}$ for the [110] directions. Inspection of the unbroadened and broadened theoretical line shapes shows that the energy at which the peak of a zero-phonon HEL occurs lies very close to the energy of the emission from hot electrons with wave vectors of the type $\mathbf{k}=k(1,1,0)$. This difference (somewhat less for $I_\perp$ than for $I_\parallel$) as a result of broadening is only 0.7 meV when $E_{ex}=1.650$ eV as in Fig. 4(b), and 1.5 meV when 1.750 eV (not shown). Therefore, from theory the position of the HEL peak measured as $I_\perp$ reflects fairly well the energy of [110] emission, the deviation from the true energy of the [110] emission being towards smaller energy. Because $m_h^*\approx 10m_e^*$, about 10% of this systematic deviation will affect E_h and the remainder $|\mathbf{k}|$, introducing uncertainties of the same order as those due to the experimental resolution. Therefore, the energies of the peak maxima may be used to plot E_h versus k if one bears in mind that the dispersion obtained will be close to the true [110] dispersion, but leaning systematically toward the true [111] curve by a few 0.1 meV. For example, for $E_{ex}=1.650$ eV [Fig. 4(b)] the peak energy $E_L=1.6105$ eV, yielding $E_h=11.5$ meV. By making use of the present theoretical model for the line shape it has thus been straightforward to extract some directional information from HEL spectra.

B. The HH-dispersion between [110] and [100]

This section shows what information can be obtained from a spectrum of the *absolute difference* $I_\perp-I_\parallel$ of the zero-phonon peak of the hot (e,A^0) photoluminescence. We summarize what was recently pointed out in Ref. 5. In a geometry where the in-going and out-going photons are polarized along [100] crystallographic directions, the degree of linear polarization in the emission spectra is theoretically predicted as $\eta_{[100]}=\frac{1}{3}$, $\eta_{[110]}=\frac{1}{11}$, and $\eta_{[111]}=0$ and thereby identifies emission from electrons with specific $\mathbf{k}$ directions (cf. Sec. II). Because $\eta_{[100]}>\eta_{[110]}$, the overall difference spectrum $I_\parallel-I_\perp$ comprises emission to a large extent from [100] electrons and to a lesser extent emission from [110] electrons, both contributions being broadened by emission from electrons traveling along other directions. Because $\eta_{[111]}=0$, no emission at all will be present from [111] electrons. Figure 5 shows such an absolute difference spectrum $I_\parallel-I_\perp$ obtained from the original spectra in Fig. 4(a). The position of the maximum in $I_\parallel-I_\perp$ is redshifted by 2.5 meV with respect to the maxima of its constituents, either $I_\parallel$ or $I_\perp$. The magnitude of this shift depends on and increases with wave vector (it is 6 meV when $E_{ex}=1.750$ eV). Since these difference spectra are due to electrons with large $\mathbf{k}$ components along one particular direction, namely [100], and none from [111] electrons, the energy of the maximum difference $I_\parallel-I_\perp$ represents a measure of the anisotropy of the hole band. Emission from [100] electrons will account mostly for the lower-energy portion of the overall $I_\parallel-I_\perp$ intensity, emission from [110] electrons mostly for the higher-energy end of the difference spectrum. The hole energy E_h obtained from its maximum, therefore, represents some average over $E_{h,[100]}$ and $E_{h,[110]}$ of unknown weights. From such measurements with different E_{ex} it is thus possible to plot an $E_h(\mathbf{k})$ curve that will lie in between the true [100] and the true [110] dispersions, and probably closer to the first. Note that here $\mathbf{e}$ and $\mathbf{e}'$ are aligned with [100] crystal axes: in this geometry the dispersion between [100] and [110] was obtained. Analogous arguments show[5] that when the polarizations are aligned with [110] axes, one obtains a dispersion curve between [110] and [111].

C. The HH-dispersion closer to [100]

Here we discuss the difference spectrum $I_\parallel-I_\perp$ obtained after the $I_\perp$ spectrum has been *normalized* to the $I_\parallel$ spectrum at its maximum. It was seen in the preceding section that the difference $I_\parallel-I_\perp$ of the original spectra contains the [100] emission on its low-energy side, and in Sec. IV A that the [110] directions account for the

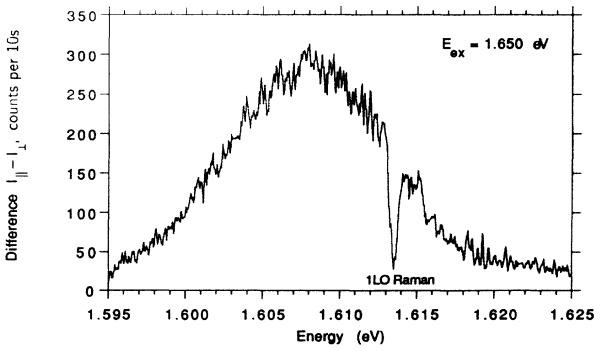

FIG. 5. Difference $I_\parallel-I_\perp$ of the original spectra in Fig. 4(a). This signal contains no contribution from electrons with $\mathbf{k}\|[111]$, a large contribution from electrons with $\mathbf{k}\|[100]$ and some from electrons with other orientations of $\mathbf{k}$ (when $\mathbf{e},\mathbf{e}'\|[100]$), but the exact proportions are unknown. The shift of the maximum of $I_\parallel-I_\perp$ with respect to the maxima of its constituents is a direct measure of some of the anisotropy of the HH valence band.

emission near the maximum of the HEL peak. Therefore, by first normalizing the HEL profiles at their maxima and subsequently subtracting (i.e., $I_{\parallel,n}-I_{\perp,n}$) a larger fraction of the luminescence emitted by hot [110] electrons may be eliminated than by taking the difference of the original spectra $I_{\parallel}-I_{\perp}$. The relative content of [100] emission is thus significantly increased in Fig. 6, which shows the difference $I_{\parallel,n}-I_{\perp,n}$ obtained in this way from both the measured and calculated original spectra in Fig. 4. The theoretical and measured maximal differences $I_{\parallel,n}-I_{\perp,n}$ in this figure are redshifted considerably with respect to the maxima in the original spectra (by more than in Fig. 5): by (4.6 ± 1) meV for $E_{ex}=1.650$ eV and, not shown, by (9.8 ± 2) meV for $E_{ex}=1.750$ eV. The main source of error is the spectral resolution; moderate laser power fluctuations do not affect the position of the maximum difference $I_{\parallel}-I_{\perp}$. Thus a further, and better, measure of the HH anisotropy is provided: one obtains from the measured maximum in Fig. 6 a point $E_h(\mathbf{k})$ which still lies between the true [100] and the true [110] HH dispersions, but considerably closer to [100] than with any of the previous methods. However, it is still not known quantitatively how distant the resulting curve is from the true [100] dispersion.

D. The HH-dispersion along the [100] and [111] directions

In this section we demonstrate how the HH dispersion may be obtained from hot (e,A^0) PL not merely close to but actually along specific high-symmetry directions. The idea is to plot, as in Fig. 7, the degree of linear polarization $\eta(E)$ as a function of luminescence energy across the first HEL peak in the cascade, both from theory and from measurement, and to relate characteristic features in these graphs to emission from carriers with specific $\mathbf{k}$ directions.

When $\eta(E)$ is calculated from the unbroadened profiles of Fig. 4(b) given by the full 16×16 $\mathbf{k}\cdot\mathbf{p}$ calculation, the dashed line is obtained, similar to the results of Alekseev

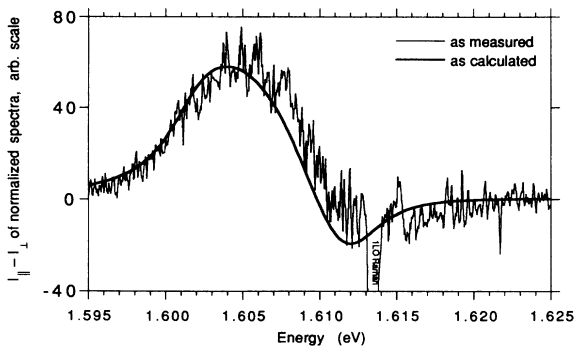

FIG. 6. Difference $I_{\parallel,n}-I_{\perp,n}$ after normalization of $I_{\parallel}$ to $I_{\perp}$ at the maximum, from the measured spectra in Fig. 4(a), and from the calculated curves in Fig. 4(b). The peak of this difference signal is at lower energy than that of the original $I_{\parallel}$ and $I_{\perp}$ spectra, and than that of the absolute difference $I_{\parallel}-I_{\perp}$ in Fig. 5, because the proportion of emission from hot electrons with $\mathbf{k}\|[100]$ is increased here, providing further information on the HH anisotropy.

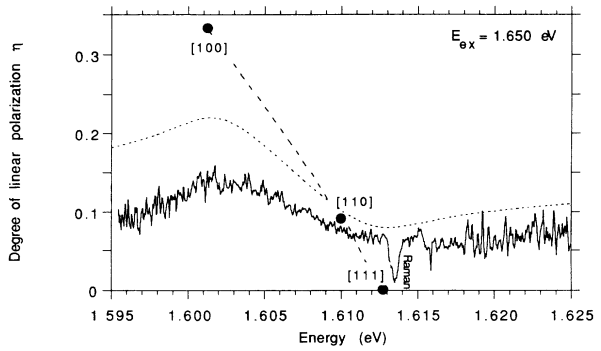

FIG. 7. Degree of linear polarization $\eta(E)$ as defined in the text and using the data of Fig. 4. Dashed: from the calculated unbroadened profile; the ●'s mark the positions corresponding to emission from k values lying along the principal crystallographic directions. Dotted: from the calculated broadened profile. Continuous: from the measured spectra $I_{\parallel}$ and $I_{\perp}$. The positions of the maximum and minimum of $\eta(E)$ label the emission from [100] and [111] carriers: markers indicate the theoretical position, which are slightly shifted by the line broadening. Thus the extrema in the measured graph identify the emission from carriers with $\mathbf{k}$ purely along those directions, if this shift is taken into account (see text for discussion).

et al.[14] Its extremal values $\eta=\frac{1}{3}$ and $\eta=0$ identifies that part of the unbroadened spectrum which is due to carriers with $\mathbf{k}$ purely along the [100] and [111] directions, and $\eta=1/11$ identifies that due to [110] carriers (black markers). When $\eta(E)$ is drawn from the calculated broadened profiles of Fig. 4(b), the dotted curve results: the two mentioned extrema of $\eta(E)$ persist as a maximum and as a minimum (from the [100] and [111] emission, respectively), but due to the broadening they have moved slightly toward each other. These features are also observed when $\eta(E)$ is drawn directly from the measured spectra in Fig. 4(a), shown here as the continuous line, with the maximum well resolved. Note that any experimental drift in the relative intensity of the $I_{\parallel}$ and $I_{\perp}$ spectra would merely shift the $\eta(E)$ curves on the y axis. From theory, we know that the maximum $\eta_{\max,\mathrm{th}}$ of the theoretical $\eta(E)$ (dotted line) labels the luminescence from electrons with $\mathbf{k}\|[100]$, except for the broadening induced shift: therefore, the maximum $\eta_{\max,\mathrm{exp}}$ labels the position of the energy axis of emission specifically from electrons with $\mathbf{k}\|[100]$, provided the broadening induced shift is taken into account. A measure of this shift (to within ≈0.1 meV) is provided by the energy difference $\Delta\eta_{\max,\mathrm{th}}$ between the two theoretical maxima from the unbroadened and broadened profiles. Then $E_{L,[100]}=E(\eta_{\max,\mathrm{exp}})-\Delta\eta_{\max,\mathrm{th}}$ yields the energy $E_{L,[100]}$ of the emission line specifically from [100] electrons. In the example of Fig. 7 for $E_{ex}=1.650$ eV one finds $E(\eta_{\max,\mathrm{exp}})=1.6027$ eV, $\Delta\eta_{\max,\mathrm{th}}=0.4$ meV, and $E_{L,[100]}=1.6023$ eV, which yields the point $E_h(\mathbf{k}\|[100])=20.0$ meV on the HH dispersion along specifically the [100] direction. Thus it has become possible to resolve the heavy-hole band quantitatively and for exactly specifiable crystal directions from hot (e,A^0) luminescence spectroscopy.

In an analogous manner, a point on the HH dispersion along specifically [111] is obtained by identifying the *minimum* of the measured $\eta(E)$ curve with luminescence from [111] carriers and correcting for the broadening induced shift through $E_{L,[111]}=E(\eta_{\min,\exp})+\Delta\eta_{\min,th}$. In Fig. 7, this minimum is near the Raman dip but not resolved with satisfactory accuracy here. It is more difficult to obtain the dispersion along [110], since this direction is not labeled by any prominent feature in the $\eta(E)$ graph. However, one way is the following. Let $E_{[100],th}$, $E_{[111],th}$, and $E_{[110],th}$ be the energies (markers in Fig. 7) of the theoretically calculated emission lines from electrons with $\mathbf{k}$ along the direction of the subscripts. Then the ratio $(E_{[111],th}-E_{[110],th})/(E_{[110],th}+E_{[100],th})$ (about 0.3) locates the [110] emission with respect to the other two emission lines, which in turn are quantities obtainable from the measured $\eta(E)$ curve in the manner indicated above.

E. Summary

The four methods given in Sec. IV A–IV D for obtaining heavy-hole dispersion curves $E_h(\mathbf{k})$ along approximate and exact high-symmetry directions in $\mathbf{k}$ space are summarized here, and the results obtained with each method are displayed in Fig. 8 and compared with related work.[5] Also included in the figure to guide the eye are parabolae with $m^*_{[100]}=0.388m_0$, $m^*_{[110]}=0.656m_0$, and $m^*_{[111]}=0.92m_0$, obtained from nonlocal pseudopotential calculations.[15]

In Sec. IV A, theory showed that the maximum of an HEL zero-phonon peak occurs at approximately the same luminescence energy as the emission from hot electrons traveling along [110] directions. The resulting HH energies are represented in Fig. 8 as closed squares and are expected to lie close to and above the true [110] dispersion. In Sec. IV B, the absolute difference $I_\parallel-I_\perp$ of measurements with $\mathbf{e},\mathbf{e}'\|[100]$ gave data points on a curve expected to lie between the [110] and [100] dispersion: the closed circles. In Sec. IV C, the difference between spectra $I_\parallel$ and $I_\perp$ after normalization at their peaks gave a curve also between the true [110] and [100] dispersions, but significantly closer to [100], represented by the diamonds. In Sec. IV D, it was shown that an analysis of the degree of linear polarization $\eta(E)$ can yield the dispersion along exactly the [100] direction, these data are represented by the triangles. Once the minima in $\eta(E)$ are resolved, as mentioned in Sec. IV D, the resulting data points will represent the true [111] dispersion above the closed squares. Then both extremal dispersions of the heavy-hole band will have been determined experimentally from hot (e,A^0) photoluminescence.

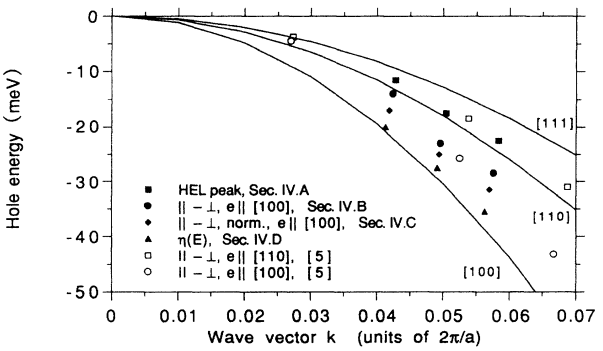

FIG. 8. Anisotropy of the heavy-hole dispersion in GaAs obtained from hot (e,A^0) luminescence, as indicated in the legend and detailed in the text. The lines are parabolas as a guide to the eye. The closed symbols are results from the present work; ■ are expected to lie close to the [110] dispersion, ● between [110] and [100], and ◆ still closer to [100]. ▲, from the degree of polarization $\eta(E)$, give the dispersion specifically along the [100] direction; all other symbols are for approximate directions. The open symbols are from Ref. 5, □, the results should lie between the true [110] and [111] dispersions, ○ between [110] and [100].

The open symbols in Fig. 8 are taken from other HEL data recently reported in Ref. 5. The open circles have the same meaning as the closed circles of this work. The open squares were obtained from an analogous set of absolute difference spectra but with $\mathbf{e},\mathbf{e}'\|[110]$; they are expected to lie between the true [110] and the true [111] curves. The data from both works are thus consistent with each other and yield complementary information.

When assessing the accuracy of the coordinates of the data in Fig. 8, one must distinguish between errors in energy, which is a measured quantity, and errors in the wave vector, for which extra input from some calculated model has to be used. The energy uncertainties of the data obtained in this work are imposed mainly by the spectral resolution, resulting in $\Delta E_h\approx\pm1$ meV at small k and somewhat larger for $k\geq0.05(2\pi/a)$. For the Kash data no errors are specified.[5] Uncertainties also arise from the determination of $|\mathbf{k}|$, for which the hot-electron energy $E_c(\mathbf{k})$ measured in this work was linked to a wave vector via the conduction-band dispersion given by Ruf and Cardona.[9] These authors find that their conduction-band dispersion agrees with that obtained from the present 16×16 $\mathbf{k}\cdot\mathbf{p}$ Hamiltonian to within a few meV. Consequently, an uncertainty in the absolute value of k of $\Delta k\approx0.003(2\pi/a)$ must be assumed, or about half of one division in Fig. 8.

In summary, Fig. 8 illustrates the progress that has been made recently in extracting directionally resolved information from hot (e,A^0) PL. It also highlights what additional interesting information is contained in such spectra ready for a systematic extraction, in conjunction with a theoretical calculation of $\eta(E)$: the dispersions along [100], [111], and also along [110] over an extended portion of the Brillouin zone.

V. THE EFFECT OF SCATTERING ON THE MOMENTUM ORIENTATION

This section briefly addresses two interesting points which Sec. III passed over: what happens to the momentum orientation within a hot-electron population when its spatial density and, therefore, the likelihood for coulombic scattering among carriers increases? And second, what happens to the momentum orientation when the entire hot-electron population is scattered by LO phonons? The analyses of the leading HEL peak carried out in Sec. IV is based on the situation in which hot-electron mo-

menta are orientated, and they can be used conversely to study the possible breakdown of such orientation. Here measurements relating to these two questions are presented. It is found that even when significant electron-electron interaction occurs, the overall orientation of the hot-electron momenta persists to a large extent. On the other hand, scattering by LO phonons seems to destroy the momentum memory of the hot-electron population.

A. Momentum orientation at high carrier density

In the preceding sections the assumption was made that the photoexcited carrier density was sufficiently small for the momentum orientation of the hot-electron population not to be disturbed significantly by carrier-carrier scattering. The agreement of the experimental data with the predictions of a model that does not include density supports this assumption. In the following we briefly investigate what effects on the hot-electron momentum distribution may be seen when their spatial density is increased by an order of magnitude.[16,17]

The measurements discussed here differ from those in Fig. 4(a) only in the density d of photoexcited carriers. One pair of spectra $I_{\parallel}$ and $I_{\perp}$ was taken at a low incident laser power density of 36 $W\,cm^{-2}$, corresponding to $d=8\times10^{14}$ cm^{-3}, and a second pair at 440 W/cm^2, corresponding to $d=9\times10^{15}$ cm^{-3}. Uncertainties of $\pm15\%$ on the carrier density result from measuring the spot size; stability of the incident power was ensured. The present *low*-density spectra are indistinguishable from the previous spectra (cf. Figs. 4–6) and are, therefore, not discussed anew.

Figure 9 shows the zero-phonon HEL peak profiles $I_{\parallel}$ and $I_{\perp}$ at the *higher* carrier density. (The inset shows the peaks before subtraction of the underlying background arising from the Boltzmann tail of the band-gap luminescence; in the absence of accurate knowledge of the band gap E_0 itself and of the intensity of the luminescence at E_0 under these conditions, the background was taken as a straight line drawn between the extremes of each spectrum, a procedure valid over such a small energy range.) In this steady state both the hot-electron and cooler carrier populations are tenfold denser, and electrostatic interaction leads to small energy exchanges within the hot-electron system. Consequently, the FWHM of this HEL peak is 2 meV larger than at low density [cf. Fig. 4(a)]. This carrier-carrier interaction must lead ultimately to a randomization of momenta. It is, therefore, interesting that in these high density $I_{\parallel}$ and $I_{\perp}$ profiles features similar to those at low density are observed, since they are characteristic of a particular momentum orientation: the intensity ratio at peak maximum $I_{\parallel}/I_{\perp}\approx1.1$, the peak shape is wider in $I_{\parallel}$ than in $I_{\perp}$, entirely due to the low energy side.

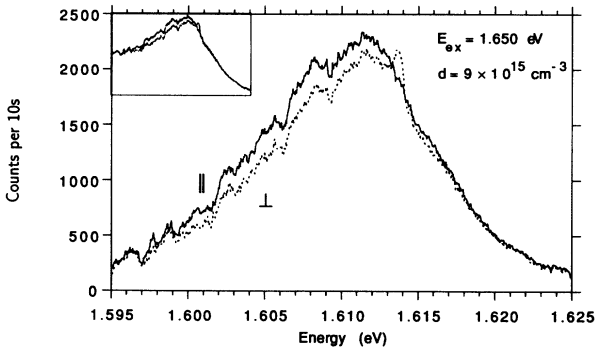

FIG. 9. The first (e,A^0) peak at the higher carrier density $d=9\times10^{15}$ cm^{-3} in $I_{\parallel}$ and $I_{\perp}$ after subtraction of a linear background due to thermalizing electrons accumulating at the bottom of the conduction band (see text). The inset shows the originals. Despite the large number of carriers present, the intensity ratio $I_{\parallel}/I_{\perp}$ and the asymmetry are comparable to those of the corresponding low-density spectra in Fig. 4(a), suggesting a broadly similar orientation of hot-electron momenta.

Figure 10 analyzes the two profiles quantitatively in some more depth. Since the *absolute* difference spectra $I_{\parallel}-I_{\perp}$ at low d and high d in Figs. 10(a) and 5 are comparable, it appears that the overall momentum distribution of hot electrons is not significantly affected by the tenfold increase in carrier density. However, this generalized statement is put into perspective by the difference of the *normalized* spectra in Fig. 10(b): as discussed in Sec. IV C, it contains a large proportion of emission from [100] electrons, and for that reason peaks at a lower luminescence energy (by 2 meV at low d) than the absolute difference. Yet at high d here its maximum is not shifted much with respect to that of the combined [100] and [110] signal in Fig. 10(a). This suggests that carrier-carrier scattering has at least partly destroyed the initial momentum orientation by eroding the proportion of [100] electrons. From Fig. 3 it seems plausible that this portion of electrons is scattered out of its initial direction, in agreement with Figs. 10(a) and 10(b). Figure 10(c) plots the degree of linear polarization $\eta(E)$ for both low- and high-density excitation. At low d (dotted) the position of η_{max} is determined by the emission line from electrons with $\mathbf{k}\|[100]$: if the interpretation of a relatively reduced hot [100] electron population at higher d is correct, then η_{max} must shift to higher energy, closer toward the center of the HEL profile. This is indeed supported by the continuously drawn $\eta(E)$ of the high d spectra, indicating the extent to which the momentum orientation has survived at high d. Note that the spectra of Fig. 10, being difference spectra, are unaffected in detail by the form of background subtracted from the peak profiles.

In conclusion, the momentum orientation of a hot-electron population has clearly been observed in linearly polarized HEL measurements despite the presence of a significant carrier density of $d=9\times10^{15}$ cm^{-3}. However, comparison with low-density measurements suggests that a partial destruction of this anisotropy has nevertheless occurred.

B. Momentum orientation after one LO-phonon emission

By contrast, emission of one LO-phonon by the electrons of a low-density population seems to be sufficient for almost complete eradication of their collective momentum orientation. The hot (e,A^0) luminescence peaks discussed so far represent the *first* peak in

the HEL cascade, i.e., before LO-phonon emission has taken place. The *second* peak in the HEL cascade, lower in energy by about $\hbar\omega_{LO}$, arises after the photoexcited electrons have each emitted one LO phonon. Measurements of $I_{\parallel}$ and $I_{\perp}$ were taken at $E_{ex}=1.700$ eV and low photoexcitation density of both the first and the second peak in the HEL cascade in the usual backscattering configuration and sample orientation. It was checked that the first peak was entirely consistent with Fig. 4(a) and the considerations made there and it is not shown here.

The second peak, after one phonon emission, is shown in Fig. 11(a). The striking feature is that the $I_{\parallel}$ and $I_{\perp}$ spectra are identical except on their low-energy slope [cf. Fig. 4(a) for contrast]. This suggests that the momenta within the hot-electron population are much less oriented than before phonon emission. The difference spectrum $I_{\parallel}-I_{\perp}$ in Fig. 11(b) of the second peak is only one half as intense as that of the first peak (not shown), and, since this subtraction is not sensitive to prior normalization, it

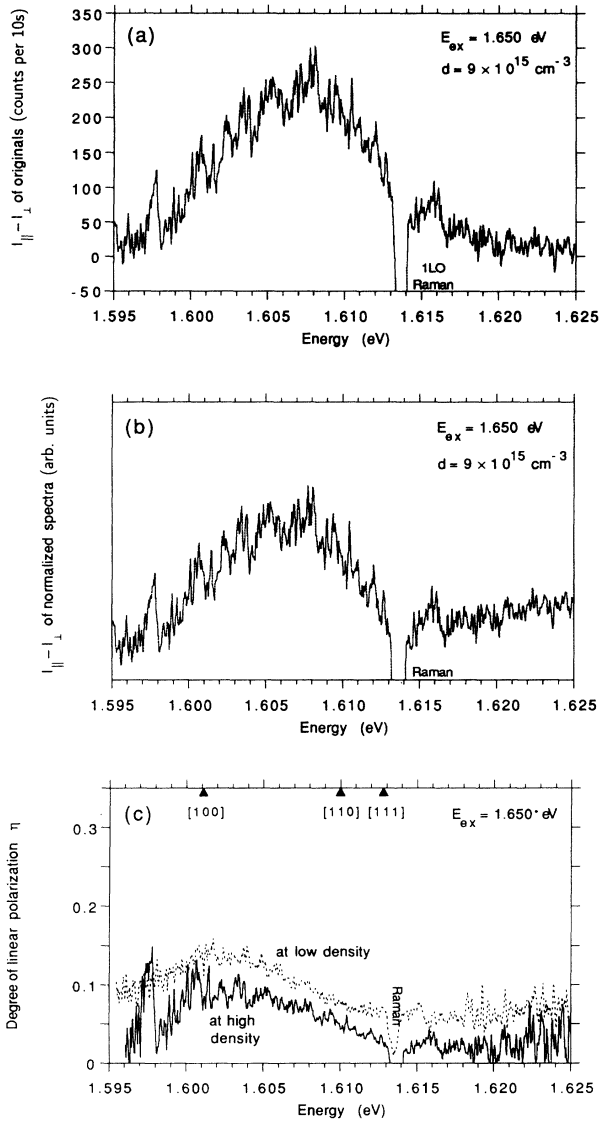

FIG. 10. (a) The similarity of the difference $I_{\parallel}-I_{\perp}$ of the high density spectra in Fig. 9 with Fig. 5 suggests the **k** distributions are broadly similar at the two densities. (b) $I_{\parallel}-I_{\perp}$ after normalization at peak. Despite a larger proportion of [100] emission than in (a) its maximum has not shifted much, and much less than at low carrier density (Fig. 6), suggesting a partial destruction of the momentum orientation along [100]. (c) Degree of polarization $\eta(E)$ in the low- and high-density spectra (cf. Figs. 7 and 9, respectively). The HEL is still clearly polarized, but the possible shift of η_{max} at high density up from its low density [100]-dominated position indicates limited randomization of **k** among the hot electrons.

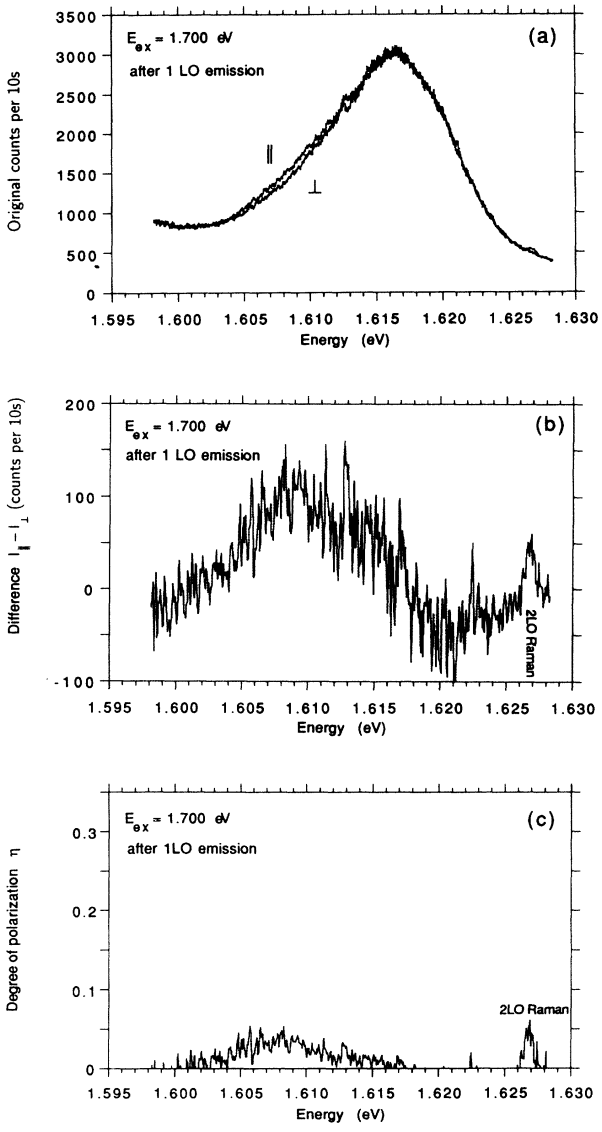

FIG. 11. (a) The original profiles of the HEL peak *after one LO emission* in $I_{\parallel}$ and $I_{\perp}$. Only the low-energy slope shows remainders of momentum orientation with [100] electrons. $T<10$ K. (b) Difference $I_{\parallel}-I_{\perp}$ of the spectra in (a). Since it is indistinguishable from the difference after normalization (not shown) no trace of the anisotropy seen in Figs. 5 and 6 prior to LO emission is observed. (c) Degree of linear polarization $\eta(E)$ exhibited in (a). Comparison with Fig. 7 shows that the degree of polarization has largely disappeared after emission of a LO phonon.

is not possible to discriminate between the emission lines of carriers with different momentum directions. This is further evidence of the breakdown by phonon emission of momentum orientation as was observed in Sec. III. It also follows that the degree of polarization $\eta(E)$, shown in Fig. 11(c), is very small on the corresponding low-energy side of the peak, and negligible elsewhere. A more detailed investigation might reveal more information on why the second peak conserves some sign of momentum orientation, and whether it too is eventually lost in the third peak, but the evidence here indicates that LO-phonon emission is an effective means of randomizing hot-electron momenta. This is quite plausible since for an electron to scatter out of its state $(E_c,\mathbf{k})$ the final state of energy $E_c-\hbar\omega_{\mathrm{LO}}$ and wave vector $\mathbf{k}+\mathbf{q}_{\mathrm{LO}}$ may, in principle, lie in any direction on the conduction-band paraboloid.

VI. CONCLUSIONS

Some properties of hot (e,A^0) photoluminescence spectra relating to the linear polarization of the exciting and detected light were studied in GaAs. The relationship between the orientation of the exciting linear electric-field vector, the hot-electron momentum, and the resulting (e,A^0) recombination spectrum is now understood and documented. A model based on a $\mathbf{k}\cdot\mathbf{p}$ band structure and on the dipole approximation was shown to predict and analyze the line shape of such spectra successfully. It is fully computable and found to yield good quantitative agreement with measurements in GaAs for hot electrons below the intervalley scattering threshold. It allows the conclusion that the systematic investigation of the phenomenon of hot-electron momentum orientation can provide detailed information on the band structure and the dynamics of hot electrons.

Applying this new understanding, two scattering processes were investigated with respect to their effect on the momentum orientation within the hot-electron population. The evidence available suggests that even in a density regime of significant carrier-carrier scattering the overall orientation of the hot-electron momenta remains largely unperturbed. On the other hand, the momentum memory of a hot-electron population appears to be eradicated to a large extent by the emission of only one LO phonon.

It was also demonstrated how the knowledge gained about the spectral composition of the (e,A^0) emission in terms of the $\mathbf{k}$ direction of the recombining hot electrons can be used to obtain directionally resolved information on the dispersion of the heavy-hole band. Various techniques were presented to obtain data points $E_h(\mathbf{k})$ approximately along or between the dispersion curves along high-symmetry crystal directions. One method, involving the measurement and the detailed calculation of the degree of linear polarization of HEL, was presented that allows the determination of the heavy-hole dispersion along *specifically* the [100], [111], and [110] directions. This and other recent progress in resolving the anisotropy of the HH band in GaAs is summarized in Fig. 8.

Potentially rewarding new areas of further work are now undoubtedly the systematic application of this knowledge to plot the HH dispersion of III-V semiconductors along the said directions over a large range of $\mathbf{k}$, and to investigate the properties of hot (e,A^0) PL with respect to circular polarization quantitatively to address the phenomenon of spin alignment.

ACKNOWLEDGMENTS

The molecular-beam-epitaxy grown GaAs samples were kindly provided by H. Kano at ERATO, University of Tokyo. This work was undertaken with financial assistance by the U.K. Science and Engineering Research Council.

[1]B. P. Zakharchenya, D. N. Mirlin, V. I. Perel', and I. I. Reshina, Usp. Fiz. Nauk **136**, 459 (1982) [Sov. Phys. Usp. **25**, 143 (1982)].

[2]G. Fasol, W. Hackenberg, H. P. Hughes, K. Ploog, E. Bauser, and H. Kano, Phys. Rev. B **41**, 1461 (1990).

[3]W. Hackenberg and G. Fasol, Appl. Phys. Lett. **57**, 174 (1990).

[4]G. Fasol and H. P. Hughes, Phys. Rev. B **33**, 2953 (1986).

[5]J. A. Kash, Phys. Rev. B **47**, 1221 (1993).

[6]V. D. Dymnikov, M. I. Dyakonov, and N. I. Perel, Zh. Eksp. Teor. Fiz. **71**, 2373 (1976) [Sov. Phys. JETP **44**, 1252 (1976)].

[7]*Semiconductors, Group IV and III-V Compounds,* edited by O. Madelung (Springer-Verlag, Berlin, 1991).

[8]J. A. Kash, M. Zachau, M. A. Tischler, and U. Ekenberg, Phys. Rev. Lett. **69**, 2260 (1992).

[9]T. Ruf and M. Cardona, Phys. Rev. B **41**, 10 747 (1990).

[10]M. Cardona, N. E. Christensen, and G. Fasol, Phys. Rev. B **38**, 1806 (1988).

[11]B. L. Gelmont, Fiz. Tekh. Poluprovodn. **9**, 1912 (1976) [Sov. Phys. Semicond. **9**, 1257 (1976)].

[12]W. Hackenberg, G. Fasol, and H. Kano, Semicond. Sci. Technol. **7**, B26 (1991).

[13]The hump on the low-energy side of the calculated broadened HEL profile is due to a slight misrepresentation of the band anisotropy by the Luttinger parameters in the $\mathbf{k}\cdot\mathbf{p}$ calculation of Ref. 10.

[14]M. A. Alekseev, I. Ya. Karlik, I. A. Merkulov, D. N. Mirlin, Yu. T. Rebane, and V. E. Sapega, Fiz. Tverd. Tela (Leningrad) **27**, 2650 (1985) [Sov. Phys. Solid State **27**, 1589 (1985)].

[15]M. V. Fischetti and J. M. Higman, in *Monte Carlo Device Simulation: Full Band and Beyond,* edited by K. Hess (Kluwer, Boston, 1991).

[16]J. A. Kash, Phys. Rev. B **40**, 3455 (1989).

[17]W. Hackenberg, H. P. Hughes, G. Fasol, and H. Kano, in *Ultrafast Laser Probe Phenomena in Semiconductors and Superconductors,* edited by R. R. Alfano, SPIE Proc. Vol. 1677 (SPIE, Bellingham, WA, 1992), p. 15.